Am J Physiol Lung Cell Mol Physiol 306: L170–L182, 2014.
First published November 8, 2013; doi:10.1152/ajplung.00167.2013.

Long-term effects of carbon containing engineered nanomaterials and asbestos in the lung: one year postexposure comparisons

Anna A. Shvedova,[1] Naveena Yanamala,[1] Elena R. Kisin,[1] Alexey V. Tkach,[1] Ashley R. Murray,[1] Ann Hubbs,[1] Madalina M. Chirila,[1] Phouthone Keohavong,[2] Lyudmila P. Sycheva,[3] Valerian E. Kagan,[2] and Vincent Castranova[1]

[1]*National Institute for Occupational Safety and Health/Centers for Disease Control and Prevention, Morgantown, West Virginia;* [2]*University of Pittsburgh, Pittsburgh, Pennsylvania;* [3]*Sysin Research Institute of Human Ecology and Environmental Health, Moscow, Russia*

Submitted 28 June 2013; accepted in final form 3 November 2013

Shvedova AA, Yanamala N, Kisin ER, Tkach AV, Murray AR, Hubbs A, Chirila MM, Keohavong P, Sycheva LP, Kagan VE, Castranova V. Long-term effects of carbon containing engineered nanomaterials and asbestos in the lung: one year postexposure comparisons. *Am J Physiol Lung Cell Mol Physiol* 306: L170–L182, 2014. First published November 8, 2013; doi:10.1152/ajplung.00167.2013.—The hallmark geometric feature of single-walled carbon nanotubes (SWCNT) and carbon nanofibers (CNF), high length to width ratio, makes them similar to a hazardous agent, asbestos. Very limited data are available concerning long-term effects of pulmonary exposure to SWCNT or CNF. Here, we compared inflammatory, fibrogenic, and genotoxic effects of CNF, SWCNT, or asbestos in mice 1 yr after pharyngeal aspiration. In addition, we compared pulmonary responses to SWCNT by bolus dosing through pharyngeal aspiration and inhalation 5 h/day for 4 days, to evaluate the effect of dose rate. The aspiration studies showed that these particles can be visualized in the lung at 1 yr postexposure, whereas some translocate to lymphatics. All these particles induced chronic bronchopneumonia and lymphadenitis, accompanied by pulmonary fibrosis. CNF and asbestos were found to promote the greatest degree of inflammation, followed by SWCNT, whereas SWCNT were the most fibrogenic of these three particles. Furthermore, SWCNT induced cytogenetic alterations seen as micronuclei formation and nuclear protrusions in vivo. Importantly, inhalation exposure to SWCNT showed significantly greater inflammatory, fibrotic, and genotoxic effects than bolus pharyngeal aspiration. Finally, SWCNT and CNF, but not asbestos exposures, increased the incidence of K-ras oncogene mutations in the lung. No increased lung tumor incidence occurred after 1 yr postexposure to SWCNT, CNF, and asbestos. Overall, our data suggest that long-term pulmonary toxicity of SWCNT, CNF, and asbestos is defined, not only by their chemical composition, but also by the specific surface area and type of exposure.

nanoparticles; long-term postexposure; inflammation; fibrosis; genotoxicity

SINGLE-WALLED CARBON NANOTUBES (SWCNT), composed of a rolled-up cylindrical sheet of graphene, and carbon nanofibers (CNF), formed from stacked graphene nanocones, are carbonaceous nanoparticles sharing fibrous morphology with a well-known, naturally occurring, toxic fiber, asbestos. Both short- and long-term outcomes of pulmonary exposure to asbestos, ranging from inflammation and fibrosis to mesothelioma and lung cancer, are well described. The hallmark geometric feature of individual SWCNT and CNF particles, high aspect ratio, makes them similar to asbestos fibers. However, chemical composition, physical dimensions, and mechanical and surface properties of SWCNT and CNF are very different from asbestos. Thus it remains uncertain whether SWCNT and CNF would follow the asbestos toxicity paradigm.

Acute and subchronic (up to 28 or 90 days) consequences of pulmonary exposure to SWCNT and CNF have been previously reported (15, 34, 46, 67, 68), where SWCNT, CNF, and asbestos have been shown to induce inflammation and fibrosis. Notably, morphological features of acute and subchronic inflammatory response to SWCNT were different from those seen after asbestos or CNF exposure. Foci of granulomatous lesions and collagen deposition were associated with dense particle-like SWCNT agglomerates, whereas no granuloma formation was found following exposure to nonagglomerated fiber-like CNF or asbestos (15, 46).

Malignant consequences of asbestos exposure are lung cancer and mesothelioma formation. High biopersistence, pulmonary penetration, fibrous morphology, the ability to generate reactive oxygen species (66, 77), as well as inflammatory and genotoxic effects associated with these phenomena or occurring independently have been implicated in asbestos carcinogenicity (34). Several recent reports suggested that SWCNT or multi-walled carbon nanotubes (MWCNT) induced DNA damage, micronuclei formation, disruption of the mitotic spindle, and polyploidy (2, 29, 33, 34, 37, 38, 45, 50, 51, 53, 61, 62, 84, 86). We have previously shown that CNF and asbestos were capable of inducing aneugenic (chromosomal malsegregation) or clastogenic (chromosome breakage) events in human small airway epithelial cells (34). Furthermore, exposure to SWCNT has been implicated in an increased incidence of K-ras oncogene mutations in vivo in an acute inhalation study (67). Considering that genetic instability combined with chronic inflammation are important factors contributing to carcinogenicity, evaluation of genotoxic effects of carbonaceous nanoparticles in vivo represents a relevant topic of investigation.

To date, no data are available describing long-term adverse effects of pulmonary exposure to SWCNT or CNF. Thus direct comparison of chronic effects of SWCNT, CNF, and asbestos conducted under the same experimental conditions in vivo is of significant importance. The present study aimed to assess inflammatory, fibrogenic, and genotoxic effects of CNF, SWCNT, and asbestos in mice 1 yr after a single pulmonary exposure by pharyngeal aspiration. We provide evidence that, up to 1 yr after exposure, SWCNT, CNF, and asbestos persist in the lung and regional lymphatics and elicit genotoxic effects and pulmonary fibrosis. To address the concerns raised about the

Address for reprint requests and other correspondence: A. A. Shvedova, NIOSH, CDC, 1095 Willowdale Rd., Morgantown, WV 26505 (e-mail: ats1@cdc.gov).

relevance of the high dose rate after bolus instillation animal exposure, we also compared the data obtained from inhalation and pharyngeal aspiration protocols for SWCNT at 1 yr post-exposure.

MATERIALS AND METHODS

Animals. Specific pathogen-free adult female C57BL/6 mice (8–10 wk) were supplied by Jackson Laboratory (Bar Harbor, ME) and weighed 20.0 ± 1.9 g when used. C57BL/6 mice were chosen for this study because of their *1*) moderate sensitivity to pulmonary fibrosis (16, 81) upon exposure to well-studied fibrogenic particles like asbestos, crystalline silica; *2*) full immuno-competence (1, 65); *3*) wide use in toxicological studies; and *4*) availability of different genetically modified variants for future mechanistic studies. Animals were housed one mouse per cage receiving HEPA-filtered air in the AAALAC-accredited NIOSH animal facility. All animals were acclimated in the animal facility under controlled temperature and humidity for 1 wk before use. Beta Chips (Northeastern Products, Warrensburg, NY) were used for bedding, which was changed weekly. Animals were supplied with water and certified chow 7913 (Harlan Teklad, Indianapolis, IN) ad libitum, in accordance with guidelines and policy set forth by the Institute of Laboratory Animals Resources, National Research Council. All experimental procedures were conducted in accordance with a protocol approved by the NIOSH Institutional Animal Care and Use Committee.

Experimental design. C57BL/6 mice were exposed to CNF (40 and 120 μg/mouse), asbestos (120 μg/mouse), or SWCNT (40 μg/mouse) via pharyngeal aspiration. The 40 μg/mouse dose has been previously demonstrated by our laboratory to cause significant alveolar interstitial fibrosis without overwhelming the lung (43, 68). For CNF, doses of 40 and 120 μg/mouse were used to range-find the response. The high dose of asbestos (120 μg/mouse) was used to compensate for the higher fiber count/mass of SWCNT vs. asbestos. The corresponding control mice were administered sterile Ca^{+2} + Mg^{+2}-free phosphate-buffered saline (PBS) vehicle. Additional mice were also exposed by inhalation to SWCNT (5 mg/m^3, 5 h/day, for 4 days, lung burden of 5 μg), whereas control mice received filtered air. These mice were exposed in whole body inhalation exposure chambers with individual steel mesh compartments as previously described (67). All mice were killed 1 yr following the last exposure. Inflammation was evaluated by total cell counts, cell differentials, and accumulation of cytokines in the bronchoalveolar lavage (BAL) fluid. Pulmonary toxicity was assessed by elevation of lactate dehydrogenase (LDH) activity and protein concentration in acellular BAL fluid. Fibrogenic responses to exposed materials were assessed by collagen deposition.

Particles. CNF were obtained from Pyrograf Products. Carbon nanofibers were vapor grown (PR-24, LHT grade) and heat treated (up to 3,000°C) to graphitize chemically vapor-deposited carbon present on the surface of the pyrograf and to remove the iron catalyst. SWCNT (Unidym, Sunnyvale, CA) were manufactured using the high-pressure CO disproportionation process (HiPco) and purified with acid treatment to remove catalytic metal contaminants (22). A UICC standard crocidolite asbestos was utilized as a positive fiber control. Total elemental carbon and trace metal analyses were performed by the Chemical Exposure and Monitoring Branch (DART/NIOSH, Cincinnati, OH). Elemental carbon was assessed according to the NIOSH Manual of Analytical Methods (NMAM) 5040 (5), whereas trace metals were analyzed by nitric acid dissolution and inductively coupled plasma-atomic emission spectrometry (ICP-AES) following NMAM method 7300 for trace metals. Raman spectroscopy, near-infrared spectroscopy, and thermo-gravimetric analysis were used for purity assessment of HiPco SWCNT. Specific surface area was measured at −196°C by the nitrogen absorption-desorption technique (Brunauer Emmet Teller method, BET) using an SA3100 Surface Area and Pore Size Analyzer (Beckman Coulter, Fullerton, CA), and particle diameter was measured by transmission electron microscopy. Before pharyngeal aspiration, particles were ultrasonicated (30 s × 3 cycles) for improved dispersion of nanoparticles.

Generation of an aerosol of SWCNT for inhalation exposure. The generation system used to deliver respirable SWCNT structures (5 mg/m^3) at a flow rate of 10 l/min to two animal exposure chambers each containing 12 mice was described previously (3). Briefly, aerosols containing SWCNT particles were generated using an aerosol dispersion system containing a powder feeder and a knife mill. The fluidized powder feeder, designed specifically for delivering the low-density material, allowed relatively constant feed rates over a period of 6 h. A knife mill was set up to provide high shear forces to tear apart agglomerates in the bulk material. Because the aerosolized material tends to form clumps, a static discharger containing ^{210}Po strips was used to reduce the electrical charges on the particles to prevent agglomerate formation due to contact charging. Before entering the inhalation chamber, the aerosol was passed through a settling chamber, followed by an air cyclone (GK 2.69; BGI, Waltham, MA) to remove the coarse portion of the particles from the aerosol by gravitational settling and centrifugal force. The cyclone had a 50% cutoff size of 4-μm aerodynamic diameter. The feed rate, mill speed, and air flow rate were adjusted to allow a target mass concentration of 5.0 mg/m^3 in the chamber, 5 h/day for 4 days. The mean flow rate through each animal chamber was 5 l/min. The resulting SWCNT aerosol was more dispersed, i.e., less agglomerated, than the SWCNT in suspension used for pharyngeal aspiration (67, 68). This inhalation exposure resulted in a lung burden of 5 μg (67). Mice were killed 1 yr postinhalation. SWCNT concentration within the exposure chambers was monitored in real-time by a DataRAM (Thermo Fisher Scientific, Waltham, MA). Gravimetric samples were also taken every 30 min at two sites within each exposure chamber using 25-mm polyvinyl chloride filters at a flow rate of 1 l/min to calibrate the DataRAM.

Particulate aspiration. Mouse pharyngeal aspiration was used for bolus particulate administration. Briefly, after anesthetization with a mixture of ketamine and xylazine (62.5 and 2.5 mg/kg subcutaneous in the abdominal area), the mouse was placed on a board in a near vertical position and the animal's tongue extended with lined forceps. A suspension (~50 μl) of SWCNT (40 μg/mouse), CNF (40 and 120 μg/mouse), or asbestos (120 μg/mouse) prepared in PBS was placed posterior on the tongue, which was held until the suspension was aspirated into the lungs. Control mice were administered sterile Ca^{+2} + Mg^{+2}-free PBS vehicle. The mice revived unassisted after ~30–40 min. All mice in PBS, CNF, SWCNT, and asbestos groups survived this exposure procedure and exhibited no negative behavioral or health outcomes. This technique provided good distribution of particles widely disseminated in a peribronchiolar pattern within the alveolar region as was detected by histopathology (55). Mice were killed 1 yr following the exposure. To reveal long-term outcomes following SWCNT, CNF, and asbestos exposure, we used three different subsets of mice (n = 6/per each endpoint). Therefore, collection of BAL, lungs tissues for histopathology, and measurements of biochemical indices in lung homogenates were performed in separate samples obtained from different animals in experimental groups.

Obtaining BAL from mice. A subset of mice was weighed and killed with intraperitoneal injection of pentobarbital sodium (>100 mg/kg) and exsanguinated. The trachea was cannulated with a blunted 22-gauge needle, and BAL was performed using cold sterile PBS at a volume of 0.9 ml for first lavage (kept separate) and 1.0 ml for subsequent lavages. Approximately 5 ml of BAL fluid per mouse was collected in sterile centrifuge tubes. Pooled BAL cells for each individual mouse were washed in PBS by alternate centrifugation (800 *g* for 10 min at 4°C) and resuspension. Cell-free first-fraction BAL aliquots were stored at 4°C for LDH assays, whereas the remainder was frozen at −80°C until analyzed for protein and cytokine levels.

BAL cell counting and differentials. The degree of inflammatory response induced by pharyngeal aspiration of SWCNT, CNF, or asbestos was estimated by quantitating total cells, alveolar macrophages (AMs), and polymorphonuclear leukocytes (PMNs) recovered by BAL. Cell counts were performed using an electronic cell counter equipped with a cell-sizing attachment (Coulter model Multisizer II with a 256C channelizer; Coulter Electronics, Hialeah, FL). AMs and PMNs were identified by their characteristic cell shape in cytospin preparations stained with Diffquick (Fisher Scientific, Pittsburgh, PA), and differential counts of BAL cells were carried out. Three hundred cells per slide were counted.

Total protein concentration and LDH activity in the BAL fluid. Measurement of total protein in the BAL fluid was performed by a modified Bradford assay according to the manufacturer's instructions (Bio-Rad, Hercules, CA) with bovine serum albumin used as a standard. The activity of LDH was assayed spectrophotometrically by monitoring the reduction of nicotinamide adenine dinucleotide at 340 nm in the presence of lactate using a Lactate Dehydrogenase Reagent Set (Pointe Scientific, Lincoln Park, MI).

Lung lavage fluid cytokine analysis. Levels of cytokines were assayed in the acellular BAL fluid following SWCNT, CNF, or asbestos aspiration. The concentrations of TNF-α, monocyte chemoattractant protein (MCP)-1, IL-12, IL-6, IL-10, and IFN-γ (sensitivity of assay is 5–7.3 pg/ml) were determined using the BD Cytometric Bead Array Mouse Inflammation Kit (BD Biosciences, San Diego, CA).

Lung preparation for microscopic evaluation. Preservation of the lung was achieved by vascular perfusion of a glutaraldehyde (2%), formaldehyde (1%), and tannic acid (1%) fixative with sucrose as an osmotic agent (42). This method of fixation was chosen to prevent possible disturbances of the airspace distribution of deposited materials while maintaining physiological inflation levels comparable to that of the end expiratory volume. This was performed using protocols previously employed to study pulmonary effects of SWCNT (68). Briefly, animals were deeply anesthetized with an overdose of pentobarbital sodium by subcutaneous injection in the abdomen, the trachea was cannulated, and laparotomy was performed. Mice were then killed by exsanguination. The pulmonary artery was cannulated via the ventricle and an outflow cannula inserted into the left atrium. In quick succession, the tracheal cannula was connected to a 5 cmH_2O pressure source, and clearing solution (saline with 100 U/ml heparin, 350 mOsm sucrose) was perfused to clear blood from the lungs. The perfusate was then switched to the fixative. Coronal sections were cut from the lungs. The lungs were embedded in paraffin and sectioned at a thickness of 5 μm with an HM 320 rotary microtome (Carl Zeiss, Thornwood, NY).

Preparation of lung homogenates. The whole mouse lungs from a subset of mice were separated from other tissues and weighed before being homogenized with a tissue tearer (model 985-370; Biospec Products, Racine, WI) in PBS (pH 7.4) for 2 min. The homogenate suspensions were frozen at −80°C until processed.

Histopathology. Histopathological alterations were evaluated in hematoxylin and eosin-stained sections by a single board-certified veterinary pathologist (A. Hubbs) familiar with the toxicological pathology of nanoparticles using guidelines for toxicological histopathology (14). Unmasked histopathology assessment was used because unmasked evaluation is generally accepted as the most accurate method for evaluating the toxicological histopathology of new agents and because deposition of SWCNT, CNF, and asbestos are visible in tissue section, making masked evaluation impossible because exposure status is apparent during the evaluation (14). SWCNT, CNF, and asbestos were visible in light microscopic sections, and their location in cells could be identified because of their ability to strongly absorb light (25, 28). The identity of SWCNT, CNF, and asbestos in tissue section was confirmed by their presence only in the group exposed to the specific test article and by comparison with the distinctive microscopic appearance of each test article before exposure. The histopathology findings from the left and right lung and tracheobronchial lymph node of a sub-set of mice were evaluated to identify variations from normal histology. Following identification of exposure-related changes, numerical data on exposure-related inflammatory changes of the lung, pleura, and lung-associated lymph nodes were obtained using semiquantitative pathology scores reflecting the severity and distribution of morphological changes as previously described (26, 27). Briefly, slides were scored for distribution (0, none; 1, focal; 2, locally extensive; 3, multifocal; 4, multifocal and coalescent; and 5, diffuse) and severity (0, none; 1, minimal; 2, mild; 3, moderate; 4, marked; and 5, severe). The pathology score was the sum of both distribution and the severity score. A separate score was determined for the inflammation of the lung (pneumonia) and inflammation of the pleura (pleuritis), but for each of these target tissues both the left and right lung were used to determine the pathology score. The presence or absence and the pathology score for fibrosis were determined in the lungs of SWCNT and air-exposed mice in the SWCNT inhalation study in trichrome-stained sections. Lymph node inflammation (lymphadenitis) was evaluated and scored as described above in hematoxylin-stained sections of tracheobronchial lymph nodes. Additionally, the tracheobronchial lymph nodes were evaluated for the presence or absence of giant cells, and the pleura was evaluated for the presence or absence of mesothelial cell hyperplasia or cellular atypia. In mice aspirating SWCNT, CNF, and asbestos, the presence or absence of pulmonary fibrosis was determined after the histopathology assessment through the evaluation of trichrome-stained sections by a board certified pathologist at Colorado Histoprep (Fort Collins, CO). The obtained histopathology results also confirmed the seen presence of inflammation in the lungs of mice aspirating SWCNT (40 μg), CNF (40 μg), CNF (120 μg), and asbestos (120 μg).

Lung collagen measurements. Total lung collagen content was determined by quantifying total soluble collagen using the Sircol Collagen Assay kit (Accurate Chemical and Scientific, Westbury, NY). Briefly, whole lungs were homogenized in 0.7 ml of 0.5 M acetic acid containing pepsin (Accurate Chemical and Scientific, Westbury, NY) with 1:10 ratio of pepsin:tissue wet weight. Each sample was stirred vigorously for 24 h at 4°C and centrifuged, and 200 μl of supernatant was assayed according to the manufacturer's instructions.

Lung karyological assay. The karyological assay is based on the microscopic analysis and quantification of karyological end points in the smears of cells from some tissues (71). As end points of genotoxic nuclear changes, micronuclei, nuclear protrusions, and multinucleated cells were measured. Nuclear protrusions (nuclear blebs, nuclear buds) are rounded protrusions from the nucleus, clearly separated from it, located close to the nucleus, and connected by a thin bridge. Micronuclei are membrane-bound nuclear material separated from the nucleus. Multinucleated cells are cells with more than two nuclei within the cytoplasm.

Lung tissues of mice exposed to SWCNT (5 mg/m^3, 5 h/day, for 4 days) by inhalation were removed from formalin, washed in water, placed in 50% KOH for 15 h. They were washed with distilled water. The cell pellet was resuspended in water and centrifuged at 1,000 revolution/min for 10 min. Precipitate was washed and centrifuged three times. Supernatant was discarded and the cell pellet resuspended in a few remaining drops of water and spread onto slides. The slides were stained with 25% acetoorcein Merck (37°C, 1 h) and 1% light green ICN Biomedical (20°C, 1 min). One thousand pneumocytes per animal were analyzed for micronuclei and nuclear protrusions.

K-ras mutation analysis. For mutation analysis, three successive lung sections were prepared from each mouse lung tissue block, combined, and treated with xylene and ethanol to eliminate the paraffin. Each tissue sample was then used for DNA extraction, using the protocol combining proteinase digestion and phenol/chloroform extraction. DNA was recovered by ethanol precipitation and resuspension in 30 μl distilled water and kept at −20°C until analyzed. A 3-μl aliquot from each DNA sample was used for K-ras mutation

analysis, using a sensitive K-ras mutation detection method that combines nested-PCR, mutant allele enrichment by Ban I restriction enzyme digestion, and denaturing gradient gel electrophoresis to separate mutant alleles from wild-type alleles, as previously described (70). Each mutant allele was isolated from the gel and further characterized by automated sequencing to determine the nature of the mutation.

Raman spectroscopy. Assessments of SWCNTs retained in the lungs 1 yr postexposure were performed using Raman microscopy. This protocol has been successfully employed for the detection of SWCNTs in tissues and cells due to the presence of a characteristic tangential-mode G-band in their Raman spectra (4, 7). The Raman spectra were measured using a Horiba Jobin-Yvon spectrometer connected to a CCD camera and a confocal microscope with an ×80 objective. Samples were excited using a 514.5-nm laser with ~5-μm spot size and a power of 0.3 mW at the sample, giving a power density of ~15 $\mu W/\mu m^2$. These conditions were kept constant across all samples. A calibration curve was constructed to estimate the amount of SWCNT in the lung slides using standard samples of SWCNT prepared as follows: 1 mg/ml of SWCNT was dispersed in 1% pluronic 127 to give a concentration of 50 μg/ml. Various volumes were dispersed on five microscope slide wells to obtain mass-per-surface-area concentrations in the range 1.875×10^{-9} $\mu g/\mu m^2$ to 1.5×10^{-7} $\mu g/\mu m^2$. The tissue sections containing both left and right lungs ($n = 5$; one slide per mouse) were first inspected visually with a ×10 objective for dark areas that contained SWCNT. Following this, the objective was changed to ×80 magnification, and laser beam was focused until the Raman signal of the G-band reached the maximum. A spectrum for that area was collected with an exposure time of 10 s. To obtain a good signal-to-noise ratio, a total of five spectra per chosen area were collected and averaged. Finally, the intensity of the G-band was translated into mass/area concentration using the calibration curve, and this number was multiplied by the estimated area of the region measured to obtain final mass per slide. Furthermore, the total amount of SWCNTs retained in the whole lung was estimated using the formula: (mass × average volume of mouse lung/volume of tissue section on each slide). An average volume of $10 \times 5 \times 0.005$ mm^3 of lung tissue section on each slide and 520 mm^3 per mouse lung was considered for estimating the total mass in each case.

Statistics. Treatment-related differences were evaluated using one-way ANOVA, using the Dunnett's Multiple Comparisons to control and Student's unpaired *t*-test with Welch's correction for unequal variances, as appropriate. Statistical significance was considered at $P < 0.05$. Data are presented as means ± SE.

RESULTS

Particle characterization. All particles utilized in the present study were characterized for their dimensions, elemental carbon, and trace metals by electron microscopy, NMAM no. 5040, and ICP-AES, respectively (Fig. 1). Upon suspension for pharyngeal aspiration, SWCNT tended to form agglomerates ranging from nanoropes to tangled structures of μm diameter size (Fig. 1*A*) (68). In contrast, CNF and asbestos (Fig. 1, *B* and *C*) were well dispersed and stable in suspensions (46). A detailed summary of chemical characterization and particle size distributions of SWCNT, CNF, and asbestos, along with their specific surface area determined by BET are provided in Fig. 1*D*.

Characterization of pulmonary inflammation and injury. To evaluate lung injury and inflammatory responses to CNF, SWCNT, or asbestos, cell differentials, total BAL cell counts, and cell damage (LDH and protein release) were determined 1 yr following exposure to nanoparticles/fibers in C57BL/6 mice.

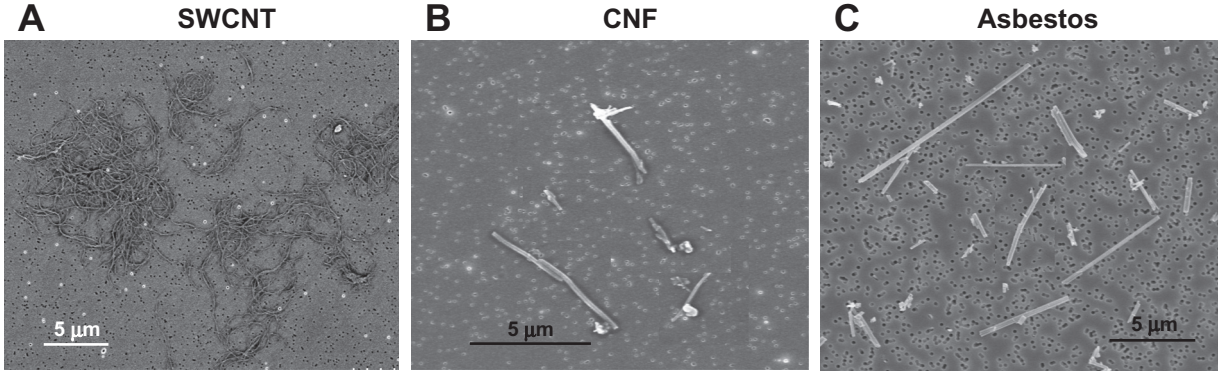

D

	SWCNT	CNF	Asbestos
Carbon Content (% wt)	99.7%	98.6%	-
Iron Content (% wt)	0.23%	1.4%	18%
Particle Diameter	~65 nm (single nanotube : 1 – 4nm)	80 – 160 nm	160 – 800 nm
Length	1 – 3 μm	5 – 30 μm	2 – 30 μm
SSA (by BET)	1040 m^2/g	35 – 45 m^2/g	8.3 m^2/g
Number of Particles/Structures (by SEM)	1.84 x 10^{-6} in 40μg	4.14 x 10^{-6} in 120μg	660 x 10^{-6} in 120μg

Fig. 1. Scanning electron micrographs of single-walled carbon nanotubes (SWCNT) (*A*), carbon nanofibers (CNF) (*B*), and asbestos (*C*) and summary of chemical and structural properties of SWCNT, CNF, and asbestos particles (*D*). SSA, specific surface area; BET, Brunauer Emmet Teller method.

Table 1. *Cellular inflammatory response 1 yr after exposure to CNF, SWCNT, or asbestos*

Cells, fold of control	SWCNT Inhalation, 5 μg	SWCNT Aspiration, 40 μg	CNF Aspiration, 40 μg	CNF Aspiration, 120 μg	Asbestos Aspiration, 120 μg
Total Cells	1.41 ± 0.08*	0.86 ± 0.15	1.40 ± 0.07*	1.55 ± 0.10*	1.33 ± 0.08*
AMs	1.38 ± 0.08*	0.85 ± 0.15	1.41 ± 0.07*	1.53 ± 0.10*	1.26 ± 0.07*
PMNs	21.71 ± 3.32*	0.95 ± 0.24	0.48 ± 0.21	2.09 ± 0.32*	5.09 ± 1.52*
Lymphocytes	2.47 ± 0.91	2.52 ± 1.06	4.79 ± 1.65*	7.31 ± 2.46*	12.58 ± 3.55*

Values are presented as means ± SE. Mice were exposed via pharyngeal aspiration with single-walled carbon nanotubes (SWCNT) (lung burden of 40 μg), carbon nanofibers (CNF) (lung burden of 40 or 120 μg), or crocidolite asbestos (lung burden of 120 μg), and by inhalation with SWCNT (lung burden of 5 μg). Animals were killed 1 yr postexposure. Data expressed as fold of control. Average cell counts in control groups from 4 independent experiments were 57.7×10^4, 56.7×10^4, 0.63×10^4, and 0.33×10^4 for total cells, alveolar macrophages (AMs), polymorphonuclear leukocytes (PMNs), and lymphocytes, respectively. $n = 6$ mice per group; $^*P > 0.05$ vs. control.

No significant cellular markers of acute inflammation were noted after SWCNT (lung burden of 40 μg) pharyngeal aspiration (Table 1). In contrast, total BAL cells, AM, and lymphocytes, as well as PMNs were significantly increased by 1.40-, 1.41- and 4.79-fold of control, respectively, upon CNF exposure at an equal mass lung burden (40 μg). Moreover, pharyngeal aspiration of CNF or asbestos at the higher mass lung burden (120 μg) induced greater elevation of all cellular markers of inflammation. In contrast to the absence of a significant cellular inflammatory response after aspiration of SWCNT, an accumulation of neutrophils (21.7-fold of control) accompanied by an elevated amount of AMs as well as lymphocytes was found after SWCNT inhalation exposure (lung burden of 5 μg).

The degree of lung permeability and injury after exposure to SWCNT, CNF, or asbestos was assessed by LDH activity (Fig. 2) and protein levels (Fig. 3) in the BAL fluid recovered from mice. Interestingly, LDH levels remained significantly elevated 1 yr postpharyngeal aspiration of 40 or 120 μg/mouse of CNF (147% or 192% of control, respectively). Pharyngeal aspiration of SWCNT (lung burden of 40 μg) or asbestos (lung burden of 120 μg) revealed low levels of total protein in BAL with the level of total protein after inhalation of SWCNT (lung burden of 5 μg) being greater than SWCNT aspiration (lung burden of 40 μg), i.e., 149% vs. 110% of control, respectively. Total protein levels remained significantly elevated in the BAL fluid after CNF (lung burden of 120 μg) pharyngeal aspiration (196% of control). In contrast, neither SWCNT nor asbestos elevated the protein concentrations in BAL fluid.

Cytokines. Chronic pulmonary inflammation in response to exposure with CNF, SWCNT, or asbestos was also monitored by measuring cytokine levels in BAL fluid (Table 2). No increase in TNF-α, IL-6, MCP-1, or IFN-γ was noted in any exposed groups. However, IL-12p70 was elevated 1 yr after pharyngeal aspiration of CNF or asbestos (lung burden of 120 μg, 230% or 285% of control, respectively), whereas neither pharyngeal aspiration nor inhalation of SWCNT induced any changes.

Collagen levels in lung tissue. Collagen accumulation in homogenized lung tissue 1 yr postexposure to CNF, SWCNT, or asbestos is shown in Fig. 4. Lung collagen was significantly increased above control in all of the pharyngeal aspiration exposure groups, with potency being SWCNT > CNF = asbestos. Notably, collagen level after inhalation of SWCNT (5-μg lung burden) was 250% of control, whereas it was 166% of control after aspiration of 40 μg of SWCNT.

Histopathology. SWCNT, CNF, and asbestos particles could all be demonstrated within tissue sections (Fig. 5). In hematoxylin and eosin-stained sections, the SWCNT were arranged as nanoropes that appeared dark olive green by light microscopy (Fig. 5*A*). Whereas the CNF were present as fibers and appeared black (Fig. 5*B*), asbestos fibers were straight and

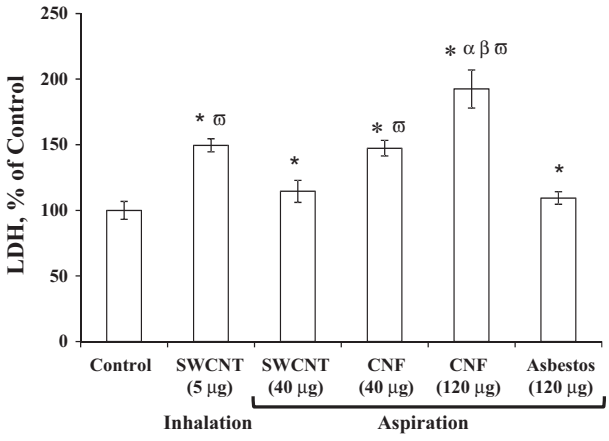

Fig. 2. Cytotoxic response to carbon nanofibers, SWCNT, or asbestos exposure. Mice were exposed via pharyngeal aspiration with SWCNT (40 μg/mouse), carbon nanofibers (40 or 120 μg/mouse), or crocidolite asbestos (120 μg/mouse), and by inhalation to SWCNT (lung burden of 5 μg). Animals were killed 1 yr postexposure. LDH, lactate dehydrogenase. Means ± SE ($n = 6$ mice per group). $^*P > 0.05$ vs. control; $^\alpha P > 0.05$ vs. CNF aspiration exposure; $^\beta P > 0.05$ vs. asbestos aspiration exposure, $^\varpi P > 0.05$ vs. SWCNT aspiration exposure.

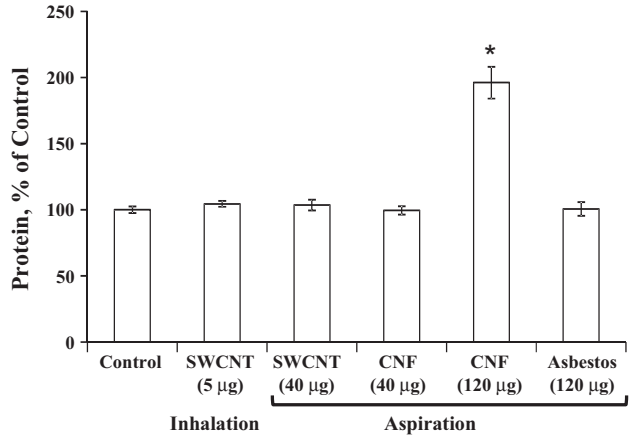

Fig. 3. The total protein concentrations of cell-free bronchoalveolar lavage (BAL) fluid in response to carbon nanofibers, SWCNT, or asbestos. Mice were exposed via pharyngeal aspiration with SWCNT (40 μg/mouse), CNF (120 μg/mouse), or crocidolite asbestos (120 μg/mouse). Animals were killed 1 yr postexposure. Means ± SE ($n = 6$ mice per group). $^*P > 0.05$ vs. control.

Table 2. *Cytokine release in BALF from mice 1 yr after exposure to CNF, SWCNT, or asbestos*

Cytokines, pg/ml	Control	SWCNT, 5 μg	SWCNT, 40 μg	CNF, 120 μg	Asbestos, 120 μg
TNF-α	0.59 ± 0.35	0.61 ± 0.03	0.49 ± 0.38	1.32 ± 0.70	1.97 ± 0.98
IL-6	14.95 ± 0.17	15.51 ± 0.92	14.46 ± 0.29	14.73 ± 0.47	15.34 ± 0.47
MCP-1	21.93 ± 0.69	29.39 ± 5.39	21.63 ± 0.29	22.10 ± 0.55	22.70 ± 0.41
IL12p70	5.51 ± 2.43	5.73 ± 0.1	3.78 ± 2.94	12.66 ± 1.66*	15.73 ± 3.08*
INF-γ	6.56 ± 0.19	7.08 ± 0.36	6.04 ± 0.14	8.79 ± 1.06	6.63 ± 0.33

Values are means ± SE. Mice were exposed via pharyngeal aspiration with SWCNT (lung burden of 40 μg), CNF, or crocidolite asbestos (lung burden of 120 μg), and by inhalation with SWCNT (lung burden of 5 μg). Animals were killed 1 yr postexposure. MCP, monocyte chemoattractant protein. $n = 6$ mice per group; $^*P > 0.05$ vs. control.

appeared gray to semitransparent by transmitted light microscopy (Fig. 5*C*).

Severity and prevalence of histopathological alterations in the lung and tracheobronchial lymph nodes of mice found 1 yr after exposure to CNF, SWCNT, or asbestos are summarized in Table 3. One year after SWCNT inhalation (5 mg/m^3, 5 h/day, 4 days; lung burden of 5 μg), the principal histopathological alterations in the lung and tracheobronchial lymph node were granulomatous bronchointerstitial pneumonia (Fig. 6*A*) and granulomatous lymphadenitis in the tracheobronchial lymph node (Fig. 7*A*). The granulomatous pneumonia in the lung was associated with foci of fibrosis in the peribronchiolar interstitium and in alveolar septa (Fig. 7*B*). This fibrosis was often in the general region where peribronchiolar lymphatics originate within the lung. SWCNT and granulomatous inflammation were present in all tracheobronchial lymph nodes examined 1 yr after inhalation (5 μg lung burden, Fig. 7*A*). In addition, giant cells, including atypical giant cells with anisokaryosis and Langhans giant cells, were seen in the lymph nodes (Fig. 7, *A* and *B*).

Granulomatous bronchointerstitial pneumonia was also seen in mice 1 yr after aspiration of SWCNT (lung burden of 40 μg), asbestos (lung burden of 120 μg), or CNF (lung burden of 40 and 120 μg). In all exposures, granulomatous inflammation and particulate material accumulated in the peribronchiolar tissue where lymphatics originate. Pleuritis, mesothelial cell hyperplasia and/or atypia, and vasculitis were seen in the mice aspirating CNF (Fig. 8). In mice 1 yr after aspiration of asbestos fibers, pleuritis, mesothelial cell hyperplasia and/or atypia, and vasculitis were also found (Fig. 9). As was noted in SWCNT-exposed mice, granulomatous lymphadenitis was also seen in mice exposed to both nanofibers and asbestos. However, asbestos fibers were generally cell associated and sometimes caused giant cell formation in the lymph nodes (Fig. 9*B*). CNF were not associated with giant cell formation. Within the lymph node, CNF were sometimes extracellular and sometimes intracytoplasmic.

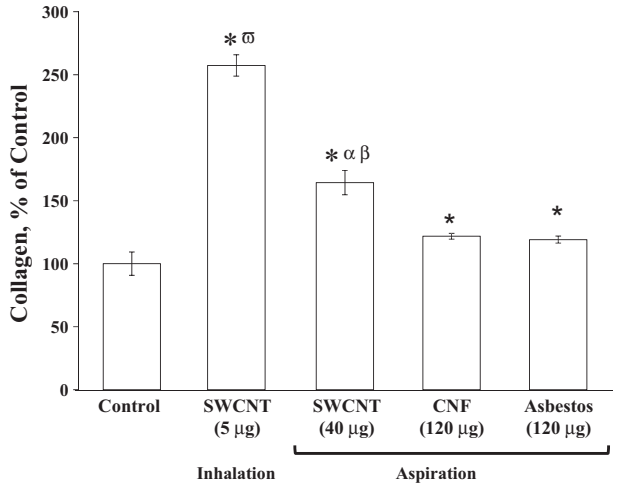

Fig. 4. Collagen accumulation in the lung 1 yr postaspiration of CNF, SWCNT, or asbestos. Mice were exposed via pharyngeal aspiration with SWCNT (40 μg/mouse), CNF (120 μg/mouse), or crocidolite asbestos (120 μg/mouse) and by inhalation to SWCNT (lung burden of 5 μg). Animals were killed 1 yr postexposure. Means ± SE ($n = 6$ mice per group). $^*P > 0.05$ vs. control; $^\alpha P > 0.05$ vs. CNF aspiration exposure; $^\beta P > 0.05$ vs. asbestos aspiration exposure; $^\varpi P > 0.05$ vs. SWCNT aspiration exposure.

K-ras mutations. To assess fiber-induced genotoxicity in C57BL/6 mice, accumulation of K-ras mutations in lungs exposed to CNF, SWCNT, or asbestos was evaluated (Fig. 10). The increase in mutation incidents observed 1 yr after inhalation of SWCNT (lung burden of 5 μg) was greater than SWCNT aspiration (lung burden of 40 μg), i.e., 33% vs. 20% over controls, respectively. Interestingly, SWCNT exposure (aspiration) induced a double mutation at *codons 12* and *8* that consisted of a GGT (glycine) to GAT (aspartate at *codon 12*) and a GTG (valine) to ATG (methionine at *codon 8*). At an equal mass lung burden (40 μg), aspiration of CNF did not induce K-ras mutations; however, exposure with lung burden of 120 μg increased the occurrence of the mutation at *codon 12* by 50% over control. In contrast, no mutations were detected after aspiration with asbestos at an equal mass lung burden to CNF (120 μg).

Karyological assays. Genotoxicity of SWCNT was also demonstrated by a significant increase in micronuclei and micronuclei plus protrusions in lung cells evaluated 1 yr after inhalation of SWCNT (lung burden 5 μg) as shown in Fig. 11.

Raman spectra. The semiquantitative measurements of SWCNTs retained in the lungs after 1 yr post-SWCNT exposure were performed using Raman microscopy. The intensity of Raman G-band (around 1,585/cm), an intrinsic feature of carbon nanotubes, was measured to estimate the amount of SWCNTs retained in the lung tissue sections of mice exposed to SWCNTs at 1 yr postexposure. A table summarizing average amount of SWCNT per lung slide along with the number of areas employed per slide is presented in Fig. 6*D*. The semiquantitative estimations from Raman spectra suggests that ~4.1 ± 1.9 μg of SWCNTs still remain in the lungs at 1 yr postexposure (Fig. 6*D*).

DISCUSSION

Murray et al. (46) recently compared acute pulmonary responses to aspiration of SWCNT, CNF, and asbestos. However, long-term pulmonary outcomes of SWCNT and CNF

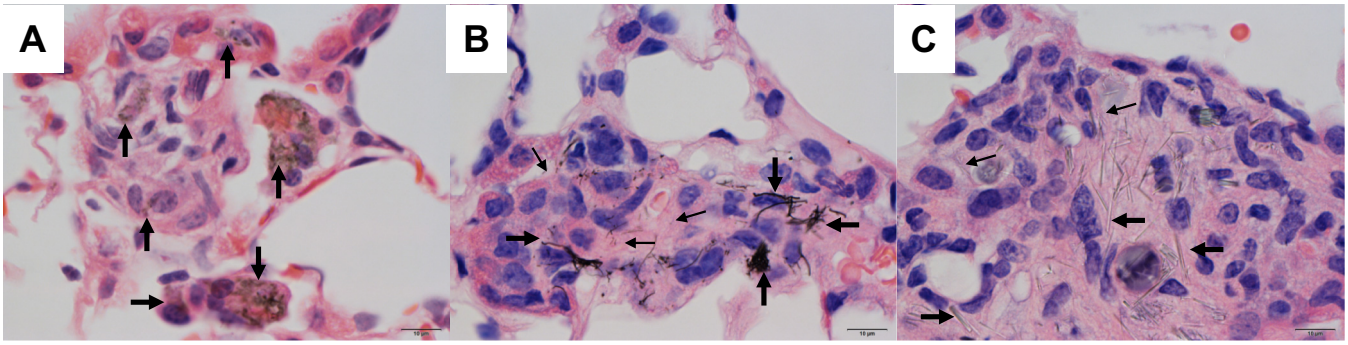

Fig. 5. Photomicrographs showing the appearance of SWCNT, CNF, and asbestos in tissue sections. *A*: SWCNT were arranged in clusters of amorphous nanoropes (arrows), which were clearly identifiable in tissue, although the individual nanotubes comprising each nanorope and the beginning and end of each nanorope could not be visualized. *B*: large CNF (large arrows) are more easily seen in tissue sections than are the smaller CNF (small arrows). *C*: asbestos fibers ranged in size from large fibers (large arrows), which were easily detectable at low magnifications, to small fibers (small arrows), which were only faintly visible at ×100 magnification.

exposure have remained largely unexplored. The present study compares, for the first time, pulmonary responses to SWCNT, CNF, and asbestos at 1 yr postexposure and establishes that SWCNT are more fibrogenic than CNF or asbestos (Fig. 4). Histopathology evaluations indicate that a substantial amount of SWCNT, CNF, and asbestos were retained in the lungs after 1 yr postexposure (Figs. 5, 7, and 8). For SWCNT, Raman microscopy showed that ~5–10% of the initial lung burden (40 μg) still remained in the lungs (Fig. 6*D*).

SWCNT, CNF, and asbestos were each identified in the tracheobronchial lymph node, suggesting that they were partially translocated to the lymphoid tissues. Whereas SWCNT and asbestos fibers were generally cell associated and sometimes caused giant cell formation in the lymph nodes, CNF were not associated with giant cell formation (Table 3). Findings of extracellular CNF within lymph nodes implied that some "stiff" nanoscale particles with high aspect ratios were transported within lymphatic fluid as opposed to the normal cell-mediated translocation of larger particles, such as asbestos (23, 24). This is consistent with the observation that small spherical nanoparticles <34 nm appear to directly enter the lymphatics (13) and suggests that this may also be true for high aspect ratio particles where one dimension is above that size range. Accumulation of SWCNT, CNF, and asbestos within lymphatics, accompanied by granulomatous lymphadenitis (Fig. 7*A*), could potentially disrupt local lymphatic clearance and induce remodeling of the affected bronchiolar-alveolar junction.

Although SWCNT induced a profound acute inflammatory response (46, 67, 68), no chronic inflammation, measured as elevated BAL levels of PMN, AM, and cytokines, was noted 1 yr after SWCNT aspiration (lung burden of 40 μg) (Tables 1 and 2). Similarly, SWCNT did not cause chronic injury to the alveolar air/blood barrier measured as protein in BAL fluid. In contrast, CNF and asbestos induced significant inflammation (BAL, PMNs, AM, IL12p70) and injury (BAL protein) although levels had declined from peak responses seen 7 days postexposure (46). This chronic response to CNF and asbestos may be due to the persistence of long fibers in lungs.

Early onset of fibrogenic response, detectable as early as 7 days postexposure to SWCNT, has been widely reported (43, 67, 68) showing two morphologically distinct features: granulomatous inflammations incorporating bundles of fibrotic connective tissue with deposits of SWCNT agglomerates, and diffuse interstitial fibrosis and alveolar wall thickening. In this study, SWCNT induced the most fibrogenicity at 1 yr postexposure, followed by CNF and asbestos, as evidenced by collagen levels in the lung (Fig. 4). Although all three particles were fibrogenic, on an equal mass lung burden basis, SWCNT were approximately fourfold higher than CNF or asbestos,

Table 3. *Prevalence of histopathological alterations in lungs and tracheobronchial lymph nodes of mice 1 yr after exposure to SWCNT, CNF, or asbestos*

Exposure, Lung burden	Pneumonia	Fibrosis	Vasculitis	Pleuritis	Mesothelial Hyperplasia/Atypia	Granulomatous Lympadenitis	Lymph Node Giant Cells
Control	0 of 10 (0 ± 0)	0 of 5 (0 ± 0)	0 of 10 (0 ± 0)	0 of 10 (0 ± 0)	0 of 10	0 of 5 (0 ± 0)	0 of 5
SWCNT, 5 μg	5 of 5 (6.00 ± 0.00)*	5 of 5 (6.6 ± 0.25)	0 of 5 0.00 ± 0.00	1 of 5 (0.6 ± 0.60)	1 of 5	4 of 4 (4.75 ± 0.63)*	2 of 4
SWCNT, 40 μg	4 of 4 (5.50 ± 0.29)*	5 of 5	2 of 4 (1.50 ± 0.96)	1 of 4 (1.00 ± 1.00)	0 of 4	ND	ND
CNF, 40 μg	5 of 5 (5.80 ± 0.20)*	4 of 5	4 of 5 (3.60 ± 0.98)*	4 of 5 (3.80 ± 1.07)*	3 of 5	5 of 5 (5.00 ± 0.55)*	0 of 5
CNF, 120 μg	5 of 5 (5.00 ± 0.00)*	4 of 6	5 of 5 (4.60 ± 0.40)*	3 of 5 (2.60 ± 1.17)*	3 of 5	5 of 5 (5.60 ± 0.40)*	0 of 5
Asbestos, 120 μg	4 of 4 (6.25 ± 0.25)*†	2 of 4	1 of 4 (1.50 ± 1.50)	3 of 4 (5.00 ± 1.68)*	4 of 4	4 of 4 (5.00 ± 0.41)*	3 of 4

Applicable values are means ± SE. Prevalence was determined for exposure-related histopathological alterations. Inflammatory changes (pneumonia, vasculitis, pleuritis, and lymphadenitis) were graded using a pathology score reflecting both the severity and distribution of the inflammation. Mice were exposed via pharyngeal aspiration with SWCNT (lung burden of 40 μg), CNF (lung burden of 40 or 120 μg), or crocidolite asbestos (lung burden of 120 μg), and by inhalation with SWCNT (lung burden of 5 μg). Animals were killed 1 yr postexposure. Data are presented as the number of positive changes among the examined samples followed parenthetically by the mean ± SE of the pathology score. 2 mice with acidophilic macrophage pneumonia (a common finding in aged mice) and 1 mouse with inadequate SWCNT aspiration were excluded from the analysis. Control mice included 5 saline controls for aspiration exposures and 5 air-exposed controls for inhalation exposures. Morphological changes in the lung of the 40-μg SWCNT group included changes morphologically consistent with heterotopic bone and osteoid (uncalcified bone matrix) formation in 3 mice. This may be associated with chronic inflammation and dystrophic calcification. *$P > 0.05$ vs. control, †$P > 0.05$ vs. CNF (lung burden of 120 μg). ND, samples not determined.

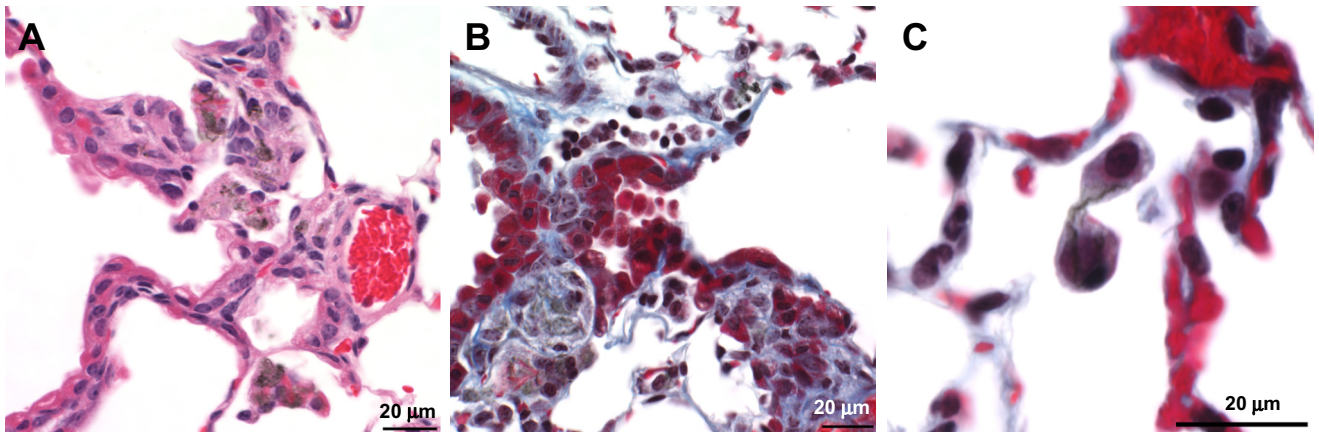

D

Sample	1	2	3	4	5
Average Mass ± SEM (ng) per slide	0.33 ± 0.03	1.02 ± 0.05	5.03 ± 0.2	1.23 ± 0.03	1.14 ± 0.03
Number of areas	4	6	9	14	11
Mass per whole lung (μg)	0.85 ± 0.08	2.66 ± 0.14	13.07 ± 0.53	3.21 ± 0.09	2.97 ± 0.07

Fig. 6. Photomicrographs of mouse lung 1 yr after inhalation of SWCNT (5 mg/m^3, 5 h/day, 4 days, lung burden 5 μg). Photomicrographs presenting bronchointerstitial pneumonia (*A*) and peribronchiolar fibrosis with intralesional SWCNT compare the sites of peribronchiolar fibrosis with the location of the mildly dilated lymphatic (*B*, top of the photomicrograph) and cytokinesis failure (*C*) in SWCNT-exposed mice. *D*: amount of SWCNT retained in the lung tissue sections in mice after 1 yr postexposure as assessed by Raman spectroscopy.

whereas CNF and asbestos were equally potent. As SWCNT directly stimulate fibroblast proliferation and collagen production (80), it is possible that SWCNT bundles form a matrix facilitating fibroblast proliferation. Furthermore, SWCNT induce profibrotic factors (TGF-β) likely promoting myofibroblast accumulation/transformation and collagen production (46).

An important issue is whether the responses to a bolus exposure are representative of responses to an equal lung burden achieved by inhalation over an extended time period. Shvedova et al. (67) compared acute pulmonary responses to SWCNT given by pharyngeal aspiration (bolus delivery) vs. 4-day inhalation exposure (1–28 days postexposure). Bolus exposure resulted in approximately fourfold less pulmonary inflammation, injury, and fibrosis compared with inhalation. This study showed the validity of this conclusion at 1 yr postexposure: inhalation exposure caused far greater chronic lung responses than bolus aspiration of SWCNT as measured by inflammation (PMNs and AMs), cell damage (LDH), and fibrosis (collagen). This difference most likely reflects the degree of agglomeration of SWCNT delivered to the lung. Shvedova et al. (67) reported that SWCNT structures were significantly more agglomerated when suspended in PBS for aspiration compared with a dry aerosol for inhalation as in the

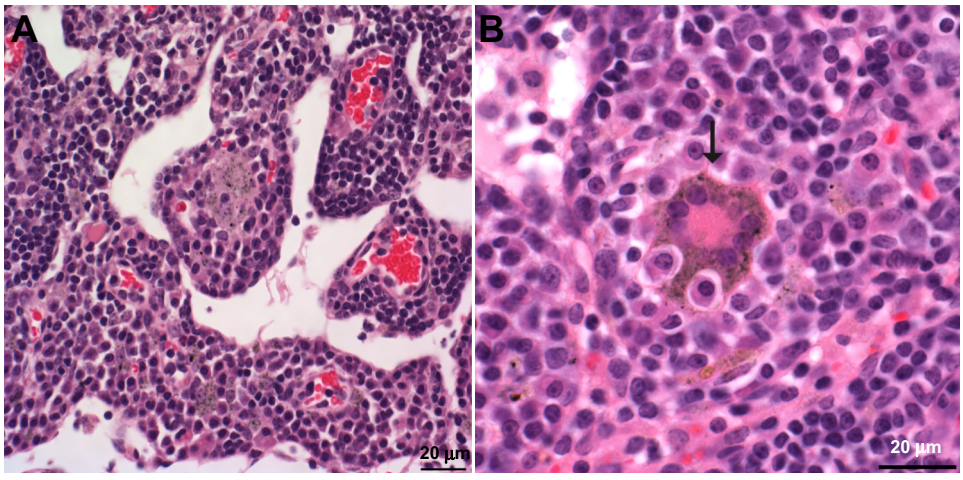

Fig. 7. Changes in the tracheobronchial lymph node 1 yr after SWCNT (5 mg/m^3, 5 h/day, 4 days, lung burden 5 μg) inhalation exposure. Photomicrographs presenting granulomatous lymphadenitis with giant cells and epithelioid macrophages containing SWCNT in the medullary cords (*A*) and Langhans giant cell (*B*) in the tracheobronchial lymph node 1 yr after SWCNT exposure.

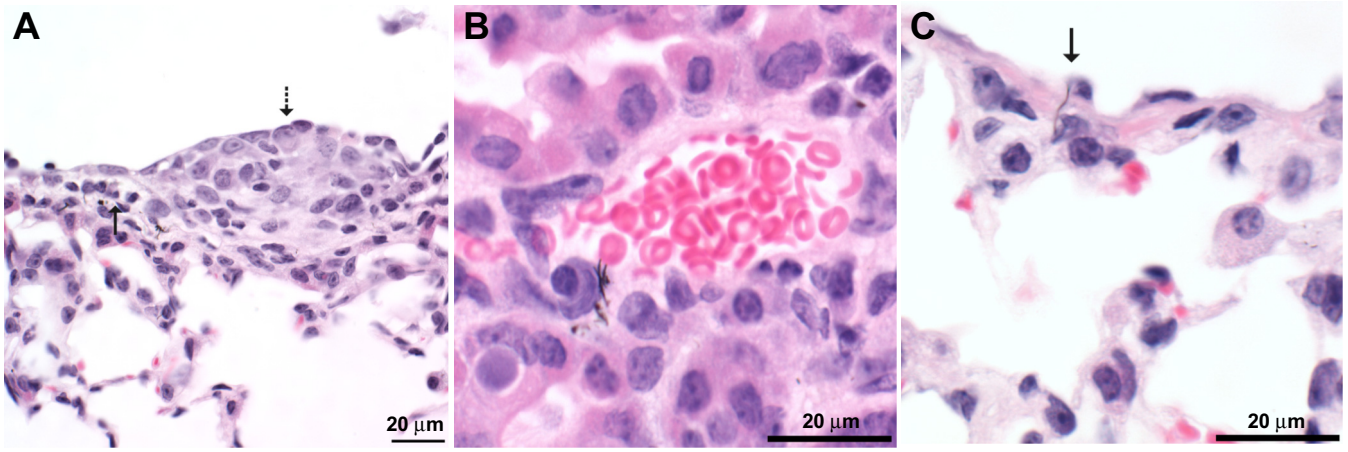

Fig. 8. Photomicrographs of mouse lung 1 yr after pharyngeal aspiration with CNF (120 μg/mouse). *A*: mesothelial cell hyperplasia (dashed arrow) and subpleural lymphangiectasia (solid arrow) in a CNF-exposed mouse. *B*: vasculitis and vascular penetration in a mouse exposed to CNF. *C*: pleural penetration in mice exposed to CNF (arrow indicating CNF penetration).

present study. In addition, Mercer et al. (43) showed that well-dispersed SWCNT are more inflammagenic and fibrogenic than less dispersed SWCNT given to mice by pharyngeal aspiration. In contrast to SWCNT, CNF and asbestos preparations used were far less agglomerated in aqueous suspensions (46). Therefore, in comparisons of the chronic fibrotic response to bolus aspiration of well-dispersed CNF and asbestos to inhalation studies of SWCNT, the fibrogenic potency of SWCNT is even more apparent. On an equal mass lung burden basis, lung collagen levels were 50-fold greater after inhalation of SWCNT compared with aspiration of CNF or asbestos. This high fibrogenic potency of SWCNT cannot be explained by the classical fiber paradigm of frustrated phagocytosis because the SWCNT preparations used in this study were very short compared with CNF and asbestos fibers (1–3 μm vs. 5–30 μm in length; Fig. 1*D*). Mercer et al. (43) proposed that the fibrogenic potential of SWCNT reflected the rate at which dispersed SWCNT translocate from alveolar airspaces to the alveolar septal interstitium. It is possible that a relatively large effective surface area of SWCNT (138 m^2/g) compared with 21 and 8.3 m^2/g for CNF and asbestos (46) could aid in the adhesion of cell/tissue proteins and lipids to the surface of SWCNT, providing an excellent scaffold for the growth and proliferation of fibroblasts (11, 12, 20, 40, 41, 80).

Chronic inflammatory response to SWCNT, CNF, and asbestos exposure presented itself as a granulomatous bronchointerstitial pneumonia, as well as pleuritis, mesothelial cell hyperplasia and/or atypia, vasculitis, and lymphadenitis (Table 3). Of note, CNF and asbestos induced more severe pleuritis compared with SWCNT where the pleuritis score was not significantly different from control (Table 3). In both asbestos- and CNF-exposed mice, pleural and vascular changes were often associated with fibers, suggesting a similarity between these particles in terms of pathological outcomes (Figs. 7*C* and 8*C*). These similarities between CNF and asbestos could be attributed to similar length (2–30 μm) and mechanical properties of these fibers, e.g., their relative stiffness and higher dispersity compared with SWCNT. In our previous study, we did not observe granuloma formation in the lung of mice exposed to CNF or asbestos up to 28 days postexposure (46). We speculate that early formation of granulomatous lesions after SWCNT, but not CNF or asbestos exposure, may be

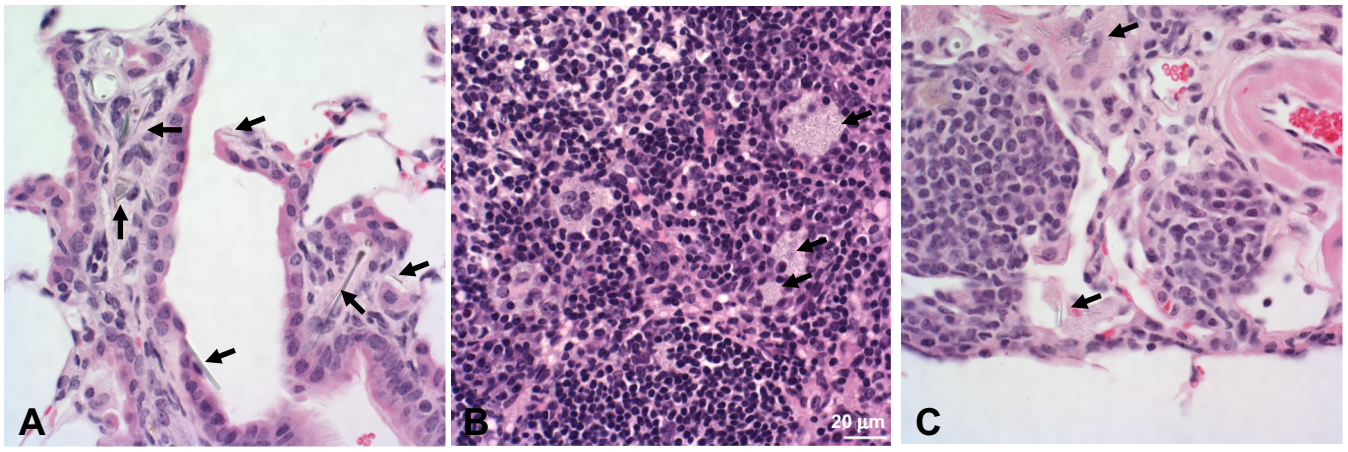

Fig. 9. Photomicrographs 1 yr after pharyngeal aspiration with asbestos (120 μg/mouse). Photomicrographs demonstrating peribronchial inflammation, fibrosis, hyperplasia (*A*), granulomatous lymphadenitis in the paracortex of the tracheobronchial lymph node (*B*), pleuritis, and lymphangiectasia (*C*) after asbestos exposure.

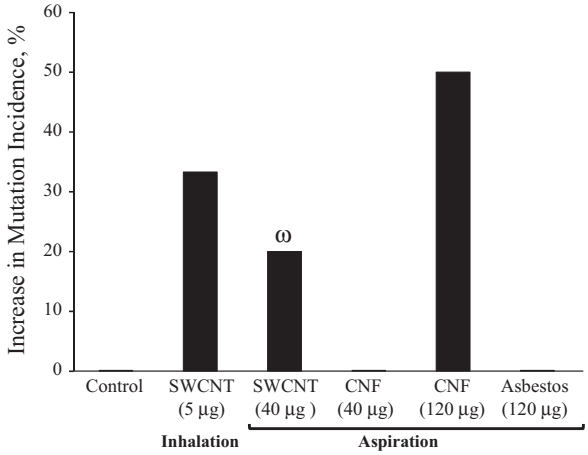

Fig. 10. Increase in the rate of K-ras mutations 1 yr after exposure of CNF, asbestos, or SWCNT. Mice were exposed via pharyngeal aspiration with SWCNT (40 μg/mouse), CNF (40 or 120 μg/mouse), or crocidolite asbestos (120 μg/mouse) and by inhalation of SWCNT (lung burden of 5 μg). Animals were killed 1 yr postexposure. ωThe double mutation contains a GGT > GAT at *codon 12* and a GTG > ATG at *codon 8* of the K-ras gene. The average numbers of mutation incidents were calculated from 3 independent experiments with 5–6 mice/group. Data are presented as an increase in the mutation incidents over control. Average rate of mutation incidents for control samples was 23 ± 14%.

attributed specifically to SWCNT agglomerates (46). Direct interference of SWCNT, CNF, or asbestos fibers with the mitotic process, abundant in repairing tissues, may result in chromosomal abnormalities and aneuploidy (64). SWCNT or MWCNT may induce DNA damage, micronuclei formation, disruption of the mitotic spindle, and polyploidy (2, 29, 33, 37, 38, 45, 50–52, 61, 62, 84, 86). Kisin et al. (34) reported that CNF, SWCNT, and asbestos were genotoxic in Chinese hamster lung fibroblast V79 cells, whereby CNF induced the same level of DNA damage as asbestos but had a stronger effect compared with SWCNT. Centromere-positive multinucleus formation was observed after CNF treatment in primary human small airway epithelial cells, indicating aneugenic potential. The present study showed that SWCNT exposure substantially increased the incidence of micronuclei and nuclear protrusions in pulmonary epithelial cells (Fig. 11). SWCNT have been shown to enter the cells (17) and reach the nucleus in interphase cells (52, 60), suggesting possible direct interactions between particles and the genetic material.

In our previous reports, we showed that SWCNT, CNF, and asbestos caused reactive oxygen species (ROS) production and oxidative stress in pulmonary cells (46, 67, 68). In this regard, asbestos fibers contained markedly higher levels of residual iron, a strong catalyst of Fenton-driven free radical oxidation, than CNF (more than 10-fold) or SWCNT (more than 70-fold). Despite this, asbestos exposure did not cause stronger long-term genotoxic effects (Fig. 10). This suggests that transition metal-catalyzed ROS production is not the major contributor to the observed genotoxic effects.

Genetic instability triggered either by inflammatory environment or continuing cycles of tissue damage/repair leading to cell metaplasia and atypia (Figs. 6–8) are the key features of carcinogenesis. K-ras oncogene is among the genes implicated in pulmonary tumorigenesis. Although K-ras may not play a critical role in the induction of mesothelioma by asbestos (47), it was frequently found in other types of lung tumors of mice exposed to chemicals (18). Previously, we reported the increased rate of SWCNT-induced K-ras mutations that took place very early after SWCNT inhalation (on *days 1–7*) and persisted through *day 28* (67). In the present study, we found an increased incidence of mutant K-ras 1 yr after exposure to SWCNT and CNF but not asbestos (Fig. 10). Inhalation exposure caused greater increase in mutation incidence than bolus aspiration of SWCNT. However, aspiration of CNF increased the rate of mutations only at the higher lung burden (120 μg), whereas no mutations were found after asbestos exposure. One of the mutations repeatedly found in SWCNT, but not in CNF-treated mice, was a double mutation at *codons 12* [GGT to GAT] and *8* [GTG to ATG] (glycine to aspartate and valine to methionine, respectively), suggesting some specificity of SWCNT effect (38).

Oncogenic K-ras mutants play a critical role in tumor initiation through induction of glucose uptake and by directing the glucose intermediates into the pentose phosphate pathway (6, 82, 85). Consistent with the function of K-ras G12D in the regulation of glycolysis (54), an increase (>1.6 fold) in glucose-6-phosphate dehydrogenase (G6PD) only upon exposure to SWCNT was reported (74). This further corroborates the phenotypic preference of the downstream signaling adapted by the K-ras G12D mutant with increased expression of G6PD via activation of phosphatidylinositol 3-kinase/Akt/mammalian target of rapamycin pathway (8). Recent results by Shvedova et al. (69) and Sargent et al. (59) suggest that SWCNT and MWCNT may act as tumor promoters. However, the appearance of tumors is defined by the balance between prooncogenic proteins and suppressors. With regards to SWCNT exposure, the enhancement of the following prooncogenic factors has been documented by proteomics studies (74): cathepsin B (CTSB) & Z (CTSZ) (30, 44, 78, 79), integrin-linked kinase (9, 49, 72), S100 calcium-binding protein A8 (S100A8) (21, 58), vimentin (56, 57, 63), and phosphoglycerate mutase 1 (10, 36, 73). However, a significant increase in potential tumor suppressors (19, 31, 48, 75, 83)–RAS-association domain family 8 (RASSF8) (~3.6-fold), B-cell CLL/lymphoma 6 member B (~3.4-fold), septin 7 (~2.5-fold), and Rho GDP dissociation inhibitor-β (ARHGDIB) (~2-fold)–was also reported in the

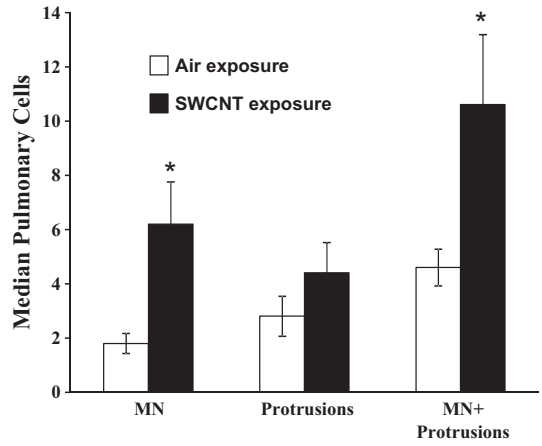

Fig. 11. Genotoxic effects of SWCNT in the lungs of mice 1 yr postinhalation exposure. Open bars, air-exposed mice; solid bars, mice inhaled SWCNT. *$P > 0.05$ vs. control. MN, micronuclei.

lungs of mice upon SWCNT exposure (74). Compatible with the lack of detectable tumors in the present study, it appears that the balance was in favor of realization of tumor-suppressing environments. Depletion of RASSF8, a candidate lung tumor suppressor gene, located on the same chromosome as K-ras gene (76), was reported to interfere with several functions leading to lung carcinogenesis (18, 32): enhanced cell proliferation and motility, disruption of cell-cell contacts, and cytoskeletal architecture (35, 39). The knockdown of RASSF8 was also associated with the development and progression of tumors as well as metastatic tendency in lung cancer (19, 39). Further investigations involving C57BL/6 and other more susceptible strains of mice are required to clarify the possible carcinogenic potential of SWCNT and CNF.

GRANTS

This work was supported by NTRC Grant 3927ZJHF (A. Shvedova), NIOSH Grant OH008282, and NIH Grants R01 ES-019304, HL-070755, and U19 AI-068021 (V. Kagan).

DISCLOSURES

The findings and conclusions in this report are those of the authors and do not necessarily represent the views of the National Institute for Occupational Safety and Health. No conflicts of interest, financial or otherwise, are declared by the authors.

AUTHOR CONTRIBUTIONS

Author contributions: A.A.S. and V.E.K. conception and design of research; A.A.S., N.Y., A.H., V.E.K., and V.C. edited and revised manuscript; A.A.S. and V.C. approved final version of manuscript; N.Y., E.R.K., A.V.T., A.H., M.M.C., and L.P.S. interpreted results of experiments; N.Y., E.R.K., A.H., and P.K. prepared figures; E.R.K., A.R.M., M.M.C., P.K., and L.P.S. performed experiments; E.R.K., A.H., M.M.C., and L.P.S. analyzed data; E.R.K., A.V.T., and V.C. drafted manuscript.

REFERENCES

1. **An CL, Gigliotti F, Harmsen AG.** Exposure of immunocompetent adult mice to *Pneumocystis carinii* f.sp muris by cohousing: growth of *P. carinii* f sp muris and host immune response. *Infect Immun* 71: 2065–2070, 2003.
2. **Asakura M, Sasaki T, Sugiyama T, Takaya M, Koda S, Nagano K, Arito H, Fukushima S.** Genotoxicity and cytotoxicity of multi-wall carbon nanotubes in cultured Chinese hamster lung cells compared with chrysotile A fibers. *J Occupat Health* 52: 155–166, 2010.
3. **Baron PA, Deye GJ, Chen BT, Schwegler-Berry DE, Shvedova AA, Castranova V.** Aerosolization of single-walled carbon nanotubes for an inhalation study. *Inhal Toxicol* 20: 751–760, 2008.
4. **Bertulli C, Beeson HJ, Hasan T, Huang YYS.** Spectroscopic characterization of protein-wrapped single-wall carbon nanotubes and quantification of their cellular uptake in multiple cell generations. *Nanotechnology* 24, 2013.
5. **Birch ME.** Elemental carbon. Monitoring of diesel exhaust particulate in the workplace. In: *NIOSH Manual of Analytical Methods (NMAM 5040)*, Chapter Q, 4th Ed. Cincinnati, OH: NIOSH, 2003.
6. **Boros LG, Lee PW, Brandes JL, Cascante M, Muscarella P, Schirmer WJ, Melvin WS, Ellison EC.** Nonoxidative pentose phosphate pathways and their direct role in ribose synthesis in tumors: is cancer a disease of cellular glucose metabolism? *Med Hypotheses* 50: 55–59, 1998.
7. **Boyer PD, Holt BD, Islam MF, Dahl KN.** Decoding membrane- versus receptor-mediated delivery of single-walled carbon nanotubes into macrophages using modifications of nanotube surface coatings and cell activity. *Soft Matter* 9: 758–764, 2013.
8. **Cespedes MV, Sancho FJ, Guerrero S, Parreno M, Casanova I, Pavon MA, Marcuello E, Trias M, Cascante M, Capella G, Mangues R.** K-ras Asp12 mutant neither interacts with Raf, nor signals through Erk and is less tumorigenic than K-ras Val12. *Carcinogenesis* 27: 2190–2200, 2006.
9. **Chen D, Zhang Y, Zhang X, Li J, Han B, Liu S, Wang L, Ling Y, Mao S, Wang X.** Overexpression of integrin-linked kinase correlates with malignant phenotype in non-small cell lung cancer and promotes lung cancer cell invasion and migration via regulating epithelial-mesenchymal transition (EMT)-related genes. *Acta Histochem* 115: 128–136, 2013.
10. **Chen G, Gharib TG, Wang H, Huang CC, Kuick R, Thomas DG, Shedden KA, Misek DE, Taylor JM, Giordano TJ, Kardia SL, Iannettoni MD, Yee J, Hogg PJ, Orringer MB, Hanash SM, Beer DG.** Protein profiles associated with survival in lung adenocarcinoma. *Proc Natl Acad Sci USA* 100: 13537–13542, 2003.
11. **Chen RJ, Bangsaruntip S, Drouvalakis KA, Kam NW, Shim M, Li Y, Kim W, Utz PJ, Dai H.** Noncovalent functionalization of carbon nanotubes for highly specific electronic biosensors. *Proc Natl Acad Sci USA* 100: 4984–4989, 2003.
12. **Chen RJ, Zhang Y, Wang D, Dai H.** Noncovalent sidewall functionalization of single-walled carbon nanotubes for protein immobilization. *J Am Chem Soc* 123: 3838–3839, 2001.
13. **Choi HS, Ashitate Y, Lee JH, Kim SH, Matsui A, Insin N, Bawendi MG, Semmler-Behnke M, Frangioni JV, Tsuda A.** Rapid translocation of nanoparticles from the lung airspaces to the body. *Nat Biotechnol* 28: 1300–U1113, 2010.
14. **Crissman JW, Goodman DG, Hildebrandt PK, Maronpot RR, Prater DA, Riley JH, Seaman WJ, Thake DC.** Best practices guideline: toxicologic histopathology. *Toxicol Pathol* 32: 126–131, 2004.
15. **Delorme MP, Muro Y, Arai T, Banas DA, Frame SR, Reed KL, Warheit DB.** Ninety-day inhalation toxicity study with a vapor grown carbon nanofiber in rats. *Toxicol Sci* 128: 449–460, 2012.
16. **Dileto CL, Travis EL.** Fibroblast radiosensitivity in vitro and lung fibrosis in vivo: comparison between a fibrosis-prone and fibrosis-resistant mouse strain. *Radiat Res* 146: 61–67, 1996.
17. **Doak SH, Griffiths SM, Manshian B, Singh N, Williams PM, Brown AP, Jenkins GJ.** Confounding experimental considerations in nanogenotoxicology. *Mutagenesis* 24: 285–293, 2009.
18. **Downward J.** Cancer: A tumour gene's fatal flaws. *Nature* 462: 44–45, 2009.
19. **Falvella FS, Manenti G, Spinola M, Pignatiello C, Conti B, Pastorino U, Dragani TA.** Identification of RASSF8 as a candidate lung tumor suppressor gene. *Oncogene* 25: 3934–3938, 2006.
20. **Fenoglio I, Greco G, Tomatis M, Muller J, Raymundo-Pinero E, Beguin F, Fonseca A, Nagy JB, Lison D, Fubini B.** Structural defects play a major role in the acute lung toxicity of multiwall carbon nanotubes: physicochemical aspects. *Chem Res Toxicol* 21: 1690–1697, 2008.
21. **Gebhardt C, Nemeth J, Angel P, Hess J.** S100A8 and S100A9 in inflammation and cancer. *Biochem Pharmacol* 72: 1622–1631, 2006.
22. **Gorelik O, Nikolaev P, Arepalli S.** Purification procedures for single-walled carbon nanotubes. *NASA Contractor Report*, NASA, 2000.
23. **Harmsen AG, Mason MJ, Muggenburg BA, Gillett NA, Jarpe MA, Bice DE.** Migration of neutrophils from lung to tracheobronchial lymph-node. *J Leukoc Biol* 41: 95–103, 1987.
24. **Harmsen AG, Muggenburg BA, Snipes MB, Bice DE.** The role of macrophages in particle translocation from lungs to lymph-nodes. *Science* 230: 1277–1280, 1985.
25. **Hubbs A, Porter DW, Mercer R, Castranova V, Sargent L, Sriram K.** Chapter 43—Nanoparticulates. In: *Haschek and Rousseaux's Handbook of Toxicologic Pathology (Third Edition)*, edited by Haschek WM, Rousseaux CG and Wallig MA. Boston, MA: Academic, 2013, pp. 1373–1419.
26. **Hubbs AF, Battelli LA, Goldsmith WT, Porter DW, Frazer D, Friend S, Schwegler-Berry D, Mercer RR, Reynolds JS, Grote A, Castranova V, Kullman G, Fedan JS, Dowdy J, Jones WG.** Necrosis of nasal and airway epithelium in rats inhaling vapors of artificial butter flavoring. *Toxicol Appl Pharmacol* 185: 128–135, 2002.
27. **Hubbs AF, Castranova V, Ma JYC, Frazer DG, Siegel PD, Ducatman BS, Grote A, SchweglerBerry D, Robinson VA, VanDyke C, Barger M, Xiang J, Parker J.** Acute lung injury induced by a commercial leather conditioner. *Toxicol Appl Pharmacol* 143: 37–46, 1997.
28. **Hubbs AF, Sargent LM, Porter DW, Sager TM, Chen BT, Frazer DG, Castranova V, Sriram K, Nurkiewicz TR, Reynolds SH, Battelli LA, Schwegler-Berry D, McKinney W, Fluharty KL, Mercer RR.** Nanotechnology: toxicologic pathology. *Toxicol Pathol* 41: 395–409, 2013.
29. **Jacobsen NR, Pojana G, White P, Moller P, Cohn CA, Korsholm KS, Vogel U, Marcomini A, Loft S, Wallin H.** Genotoxicity, cytotoxicity, and reactive oxygen species induced by single-walled carbon nanotubes and C(60) fullerenes in the FE1-Mutatrade mark Mouse lung epithelial cells. *Environ Mol Mutagen* 49: 476–487, 2008.
30. **Jedeszko C, Sloane BF.** Cysteine cathepsins in human cancer. *Biol Chem* 385: 1017–1027, 2004.

31. **Jia ZF, Huang Q, Kang CS, Yang WD, Wang GX, Yu SZ, Jiang H, Pu PY.** Overexpression of septin 7 suppresses glioma cell growth. *J Neurooncol* 98: 329–340, 2010.
32. **Katoh Y, Katoh M.** Hedgehog target genes: mechanisms of carcinogenesis induced by aberrant hedgehog signaling activation. *Curr Mol Med* 9: 873–886, 2009.
33. **Kisin ER, Murray AR, Keane MJ, Shi XC, Schwegler-Berry D, Gorelik O, Arepalli S, Castranova V, Wallace WE, Kagan VE, Shvedova AA.** Single-walled carbon nanotubes: geno- and cytotoxic effects in lung fibroblast V79 cells. *J Toxicol Environ Health A* 70: 2071–2079, 2007.
34. **Kisin ER, Murray AR, Sargent L, Lowry D, Chirila M, Siegrist KJ, Schwegler-Berry D, Leonard S, Castranova V, Fadeel B, Kagan VE, Shvedova AA.** Genotoxicity of carbon nanofibers: Are they potentially more or less dangerous than carbon nanotubes or asbestos? *Toxicol Appl Pharmacol* 252: 1–10, 2011.
35. **Langton PF, Colombani J, Chan EH, Wepf A, Gstaiger M, Tapon N.** The dASPP-dRASSF8 complex regulates cell-cell adhesion during Drosophila retinal morphogenesis. *Curr Biol* 19: 1969–1978, 2009.
36. **Li C, Xiao Z, Chen Z, Zhang X, Li J, Wu X, Li X, Yi H, Li M, Zhu G, Liang S.** Proteome analysis of human lung squamous carcinoma. *Proteomics* 6: 547–558, 2006.
37. **Li X, Peng Y, Qu X.** Carbon nanotubes selective destabilization of duplex and triplex DNA and inducing B-A transition in solution. *Nucleic Acids Res* 34: 3670–3676, 2006.
38. **Lindberg HK, Falck GC, Suhonen S, Vippola M, Vanhala E, Catalan J, Savolainen K, Norppa H.** Genotoxicity of nanomaterials: DNA damage and micronuclei induced by carbon nanotubes and graphite nanofibres in human bronchial epithelial cells in vitro. *Toxicol Lett* 186: 166–173, 2009.
39. **Lock FE, Underhill-Day N, Dunwell T, Matallanas D, Cooper W, Hesson L, Recino A, Ward A, Pavlova T, Zabarovsky E, Grant MM, Maher ER, Chalmers AD, Kolch W, Latif F.** The RASSF8 candidate tumor suppressor inhibits cell growth and regulates the Wnt and NF-kappaB signaling pathways. *Oncogene* 29: 4307–4316, 2010.
40. **Meng J, Kong H, Han Z, Wang C, Zhu G, Xie S, Xu H.** Enhancement of nanofibrous scaffold of multiwalled carbon nanotubes/polyurethane composite to the fibroblasts growth and biosynthesis. *J Biomed Mater Res A* 88: 105–116, 2009.
41. **Meng J, Yang M, Song L, Kong H, Wang CY, Wang R, Wang C, Xie SS, Xu HY.** Concentration control of carbon nanotubes in aqueous solution and its influence on the growth behavior of fibroblasts. *Colloids Surf B Biointerfaces* 71: 148–153, 2009.
42. **Mercer RR, Russell ML, Crapo JD.** Alveolar septal structure in different species. *J Appl Physiol* 77: 1060–1066, 1994.
43. **Mercer RR, Scabilloni J, Wang L, Kisin E, Murray AR, Schwegler-Berry D, Shvedova AA, Castranova V.** Alteration of deposition pattern and pulmonary response as a result of improved dispersion of aspirated single-walled carbon nanotubes in a mouse model. *Am J Physiol Lung Cell Mol Physiol* 294: L87–L97, 2008.
44. **Mohamed MM, Sloane BF.** Cysteine cathepsins: multifunctional enzymes in cancer. *Nat Rev Cancer* 6: 764–775, 2006.
45. **Muller J, Decordier I, Hoet PH, Lombaert N, Thomassen L, Huaux F, Lison D, Kirsch-Volders M.** Clastogenic and aneugenic effects of multi-wall carbon nanotubes in epithelial cells. *Carcinogenesis* 29: 427–433, 2008.
46. **Murray AR, Kisin ER, Tkach AV, Yanamala N, Mercer R, Young SH, Fadeel B, Kagan VE, Shvedova AA.** Factoring-in agglomeration of carbon nanotubes and nanofibers for better prediction of their toxicity versus asbestos. *Part Fibre Toxicol* 9: 10, 2012.
47. **Ni Z, Liu Y, Keshava N, Zhou G, Whong W, Ong T.** Analysis of K-ras and p53 mutations in mesotheliomas from humans and rats exposed to asbestos. *Mutat Res* 468: 87–92, 2000.
48. **Niu H, Li H, Xu C, He P.** Expression profile of RhoGDI2 in lung cancers and role of RhoGDI2 in lung cancer metastasis. *Oncol Rep* 24: 465–471, 2010.
49. **Okamura M, Yamaji S, Nagashima Y, Nishikawa M, Yoshimoto N, Kido Y, Iemoto Y, Aoki I, Ishigatsubo Y.** Prognostic value of integrin beta1-ILK-pAkt signaling pathway in non-small cell lung cancer. *Hum Pathol* 38: 1081–1091, 2007.
50. **Pacurari M, Yin XJ, Ding M, Leonard SS, Schwegler-Berry D, Ducatman BS, Chirila M, Endo M, Castranova V, Vallyathan V.** Oxidative and molecular interactions of multi-wall carbon nanotubes (MWCNT) in normal and malignant human mesothelial cells. *Nanotoxicology* 2: 155–170, 2008.
51. **Pacurari M, Yin XJ, Zhao J, Ding M, Leonard SS, Schwegler-Berry D, Ducatman BS, Sbarra D, Hoover MD, Castranova V, Vallyathan V.** Raw single-wall carbon nanotubes induce oxidative stress and activate MAPKs, AP-1, NF-kappaB, and Akt in normal and malignant human mesothelial cells. *Environ Health Perspect* 116: 1211–1217, 2008.
52. **Pantarotto D, Briand JP, Prato M, Bianco A.** Translocation of bioactive peptides across cell membranes by carbon nanotubes. *Chem Commun*: 16–17, 2004.
53. **Patlolla A, Knighten B, Tchounwou P.** Multi-walled carbon nanotubes induce cytotoxicity, genotoxicity and apoptosis in normal human dermal fibroblast cells. *Ethn Dis* 20: S1-65–72, 2010.
54. **Racker E, Resnick RJ, Feldman R.** Glycolysis and methylaminoisobutyrate uptake in rat-1 cells transfected with ras or myc oncogenes. *Proc Natl Acad Sci USA* 82: 3535–3538, 1985.
55. **Rao GVS, Tinkle S, Weissman DN, Antonini JM, Kashon ML, Salmen R, Battelli LA, Willard PA, Hubbs AF, Hoover MD.** Efficacy of a technique for exposing the mouse lung to particles aspirated from the pharynx. *J Toxicol Environ Health A* 66: 1441–1452, 2003.
56. **Rho JH, Roehrl MH, Wang JY.** Glycoproteomic analysis of human lung adenocarcinomas using glycoarrays and tandem mass spectrometry: differential expression and glycosylation patterns of vimentin and fetuin A isoforms. *Protein J* 28: 148–160, 2009.
57. **Richardson F, Young GD, Sennello R, Wolf J, Argast GM, Mercado P, Davies A, Epstein DM, Wacker B.** The evaluation of E-Cadherin and vimentin as biomarkers of clinical outcomes among patients with non-small cell lung cancer treated with erlotinib as second- or third-line therapy. *Anticancer Res* 32: 537–552, 2012.
58. **Salama I, Malone PS, Mihaimeed F, Jones JL.** A review of the S100 proteins in cancer. *Eur J Surg Oncol* 34: 357–364, 2008.
59. **Sargent LM, Porter DW, Lowry DT, Battelli LA, Siegrist K, Kashon ML, Chen BT, Frazer D, Staska L, Hubbs AF, McKinney W, Andrew M, Tsuruoka S, Endo M, Castranova V.** Multiwalled carbon nanotube-induced lung tumors. *Toxicologist* 132: A457, 2013.
60. **Sargent LM, Ensell MX, Ostvold AC, Baldwin KT, Kashon ML, Lowry DT, Senft JR, Jefferson AM, Johnson RC, Li Z, Tyson FL, Reynolds SH.** Chromosomal changes in high- and low-invasive mouse lung adenocarcinoma cell strains derived from early passage mouse lung adenocarcinoma cell strains. *Toxicol Appl Pharmacol* 233: 81–91, 2008.
61. **Sargent LM, Reynolds SH, Castranova V.** Potential pulmonary effects of engineered carbon nanotubes: in vitro genotoxic effects. *Nanotoxicology* 4: 396–408, 2010.
62. **Sargent LM, Shvedova AA, Hubbs AF, Salisbury JL, Benkovic SA, Kashon ML, Lowry DT, Murray AR, Kisin ER, Friend S, McKinstry KT, Battelli L, Reynolds SH.** Induction of aneuploidy by single-walled carbon nanotubes. *Environ Mol Mutagen* 50: 708–717, 2009.
63. **Satelli A, Li S.** Vimentin in cancer and its potential as a molecular target for cancer therapy. *Cell Mol Life Sci* 68: 3033–3046, 2011.
64. **Sekido Y.** Molecular biology of malignant mesothelioma. *Environ Health Prev Med* 13: 65–70, 2008.
65. **Shellito J, Suzara VV, Blumenfeld W, Beck JM, Steger HJ, Ermak TH.** A new model of Pneumocystis carinii infection in mice selectively depleted of helper T lymphocytes. *J Clin Invest* 85: 1686–1693, 1990.
66. **Shukla A, Gulumian M, Hei TK, Kamp D, Rahman Q, Mossman BT.** Multiple roles of oxidants in the pathogenesis of asbestos-induced diseases. *Free Radic Biol Med* 34: 1117–1129, 2003.
67. **Shvedova AA, Kisin E, Murray AR, Johnson VJ, Gorelik O, Arepalli S, Hubbs AF, Mercer RR, Keohavong P, Sussman N, Jin J, Yin J, Stone S, Chen BT, Deye G, Maynard A, Castranova V, Baron PA, Kagan VE.** Inhalation vs. aspiration of single-walled carbon nanotubes in C57BL/6 mice: inflammation, fibrosis, oxidative stress, and mutagenesis. *Am J Physiol Lung Cell Mol Physiol* 295: L552–L565, 2008.
68. **Shvedova AA, Kisin ER, Mercer R, Murray AR, Johnson VJ, Potapovich AI, Tyurina YY, Gorelik O, Arepalli S, Schwegler-Berry D, Hubbs AF, Antonini J, Evans DE, Ku BK, Ramsey D, Maynard A, Kagan VE, Castranova V, Baron P.** Unusual inflammatory and fibrogenic pulmonary responses to single-walled carbon nanotubes in mice. *Am J Physiol Lung Cell Mol Physiol* 289: L698–L708, 2005.
69. **Shvedova AA, Tkach AV, Kisin ER, Khaliullin T, Stanley S, Gutkin DW, Star A, Chen Y, Shurin GV, Kagan VE, Shurin MR.** Carbon nanotubes enhance metastatic growth of lung carcinoma via up-regulation of myeloid-derived suppressor cells. *Small* 9: 1691–1695, 2013.

70. **Stabile LP, Rothstein ME, Keohavong P, Jin J, Yin J, Land SR, Dacic S, Luong M, Kim KJ, Dulak AM, Siegfried JM.** Therapeutic targeting of human hepatocyte growth factor with a single neutralizing monoclonal antibody reduces lung tumorigenesis. *Mol Cancer Ther* 7: 1913–1922, 2008.
71. **Sycheva LP.** Biological value, scoring criteria and limits of variation of full spectrum karyological end points of exfoliated cells for estimation of human cytogenetic status. *J Med Genet* 11: 3–11, 2007.
72. **Takanami I.** Increased expression of integrin-linked kinase is associated with shorter survival in non-small cell lung cancer. *BMC Cancer* 5: 1, 2005.
73. **Tang CE, Li C, Xiao ZQ, Zhang XP, Chen ZC, Yi H, Li JL, Duan CJ, Liang SP.** [Comparative proteome analysis of human lung squamous cell carcinoma]. *Zhonghua Zhong Liu Za Zhi* 28: 274–279, 2006.
74. **Teeguarden JG, Webb-Robertson BJ, Waters KM, Murray AR, Kisin ER, Varnum SM, Jacobs JM, Pounds JG, Zanger RC, Shvedova AA.** Comparative proteomics and pulmonary toxicity of instilled single-walled carbon nanotubes, crocidolite asbestos, and ultrafine carbon black in mice. *Toxicol Sci* 120: 123–135, 2011.
75. **Underhill-Day N, Hill V, Latif F.** N-terminal RASSF family (RASSF7-RASSF10). A mini review. *Epigenetics* 6: 284–292, 2011.
76. **Underhill-Day N, Hill V, Latif F.** N-terminal RASSF family: RASSF7-RASSF10. *Epigenetics* 6: 284–292, 2011.
77. **Vallyathan V, Shi XL, Castranova V.** Reactive oxygen species: Their relation to pneumoconiosis and carcinogenesis. *Environ Health Perspect* 106: 1151–1155, 1998.
78. **Vasiljeva O, Papazoglou A, Kruger A, Brodoefel H, Korovin M, Deussing J, Augustin N, Nielsen BS, Almholt K, Bogyo M, Peters C, Reinheckel T.** Tumor cell-derived and macrophage-derived cathepsin B promotes progression and lung metastasis of mammary cancer. *Cancer Res* 66: 5242–5250, 2006.
79. **Wang J, Chen L, Li Y, Guan XY.** Overexpression of cathepsin Z contributes to tumor metastasis by inducing epithelial-mesenchymal transition in hepatocellular carcinoma. *PloS One* 6: e24967, 2011.
80. **Wang LY, Mercer RR, Rojanasakul Y, Qiu AJ, Lu YJ, Scabilloni JF, Wu NQ, Castranova V.** Direct fibrogenic effects of dispersed single-walled carbon nanotubes on human lung fibroblasts. *J Toxicol Environ Health A* 73: 410–422, 2010.
81. **Warshamana GS, Pociask DA, Sime P, Schwartz DA, Brody AR.** Susceptibility to asbestos-induced and transforming growth factor-beta1-induced fibroproliferative lung disease in two strains of mice. *Am J Respir Cell Mol Biol* 27: 705–713, 2002.
82. **Weinberg F, Hamanaka R, Wheaton WW, Weinberg S, Joseph J, Lopez M, Kalyanaraman B, Mutlu GM, Budinger GR, Chandel NS.** Mitochondrial metabolism and ROS generation are essential for Kras-mediated tumorigenicity. *Proc Natl Acad Sci USA* 107: 8788–8793, 2010.
83. **Xu L, Li X, Chu ES, Zhao G, Go MY, Tao Q, Jin H, Zeng Z, Sung JJ, Yu J.** Epigenetic inactivation of BCL6B, a novel functional tumour suppressor for gastric cancer, is associated with poor survival. *Gut* 61: 977–985, 2012.
84. **Yamashita K, Yoshioka Y, Higashisaka K, Morishita Y, Yoshida T, Fujimura M, Kayamuro H, Nabeshi H, Yamashita T, Nagano K, Abe Y, Kamada H, Kawai Y, Mayumi T, Yoshikawa T, Itoh N, Tsunoda S, Tsutsumi Y.** Carbon nanotubes elicit dna damage and inflammatory response relative to their size and shape. *Inflammation* 33: 276–280, 2010.
85. **Ying H, Kimmelman AC, Lyssiotis CA, Hua S, Chu GC, Fletcher-Sananikone E, Locasale JW, Son J, Zhang H, Coloff JL, Yan H, Wang W, Chen S, Viale A, Zheng H, Paik JH, Lim C, Guimaraes AR, Martin ES, Chang J, Hezel AF, Perry SR, Hu J, Gan B, Xiao Y, Asara JM, Weissleder R, Wang YA, Chin L, Cantley LC, DePinho RA.** Oncogenic Kras maintains pancreatic tumors through regulation of anabolic glucose metabolism. *Cell* 149: 656–670, 2012.
86. **Zhu L, Chang DW, Dai LM, Hong YL.** DNA damage induced by multiwalled carbon nanotubes in mouse embryonic stem cells. *Nano Lett* 7: 3592–3597, 2007.